

---

# RETHINKING THE ZIGZAG FLATTENING FOR IMAGE READING

---

A PREPRINT

 **Qingsong Zhao**

Tongji University, China

qingsongzhao@tongji.edu.cn

 **Zhipeng Zhou**

Chinese Academay of Sciences, Beijing, China

zhouzhipeng113@mails.ucas.ac.cn

 **Shuguang Dou**

Tongji University, China

2010504@tongji.edu.cn

 **Yangguang Li**

SenseTime Research, Beijing, China

liyangguang@sensetime.com

 **Rui Lu**

Tsinghua University, Beijing, China

r-lu21@mails.tsinghua.edu.cn

 **Cairong Zhao** 

Tongji University, China

zhaocairong@tongji.edu.cn

 **Yin Wang** 

Tongji University, China

yinw@tongji.edu.cn

March 16, 2022

## ABSTRACT

Sequence ordering of word vector matters a lot to text reading, which has been proven in natural language processing (NLP). However, the rule of different sequence ordering in computer vision (CV) was not well explored, e.g., why the “zigzag” flattening (ZF) is commonly utilized as a default option to get the image patches ordering in vision transformers (ViTs). Notably, when decomposing multi-scale images, the ZF could not maintain the invariance of feature point positions. To this end, we investigate the Hilbert fractal flattening (HF) as another method for sequence ordering in CV and contrast it against ZF. The HF has proven to be superior to other curves in maintaining spatial locality, when performing multi-scale transformations of dimensional space. And it can be easily plugged into most deep neural networks (DNNs). Extensive experiments demonstrate that it can yield consistent and significant performance boosts for a variety of architectures. Finally, we hope that our studies spark further research about the flattening strategy of image reading.

## 1 Introduction

Humans usually read text by row or by column, but how do you “read” a 2D image? We first look at the area of greatest interest and then the other areas or patches. And how the DNNs do with the image and text? Arguably, regardless of the text or image, many DNNs read it as text. Recently years, inspired by the Transformer extension successes in NLP, Convolution-free architectures, in particular vision Transformers Dosovitskiy et al. (2021), have become the model of choice in computer vision. A series of works try combining CNN-like architectures with Transformers, some replacing the convolutions totally Wang et al. (2021); Liu et al. (2021).

To apply Transformer from NLP to CV, however, the image embedding scale had to be reduced on account of computational cost of the Transformers would scale quadratically with the number of pixels. An image can simply be treated as  $16 \times 16$  words in ViT, but is it suitable to utilize a text-reading approach to read the images? In this work, we investigated the question of whether, fundamentally, the “zigzag” flattening strategy (aka line by line) is the optimal solution for image reading. Intuitively, the writing can be compared to a one-way time line, which ranked the key information. On the contrary, the vision system projects the static real world onto a two-dimensional screen, which constitutes the image.

The key information on the image can be considered as an undirected graph Bronstein et al. (2021). In other words, all the key information on an image can not be represented in a one-way vector. This also explains that the semantics expressed by the image is unchanged after rotation, see Fig. 2 (a) and (b). In addition, the position of the key information

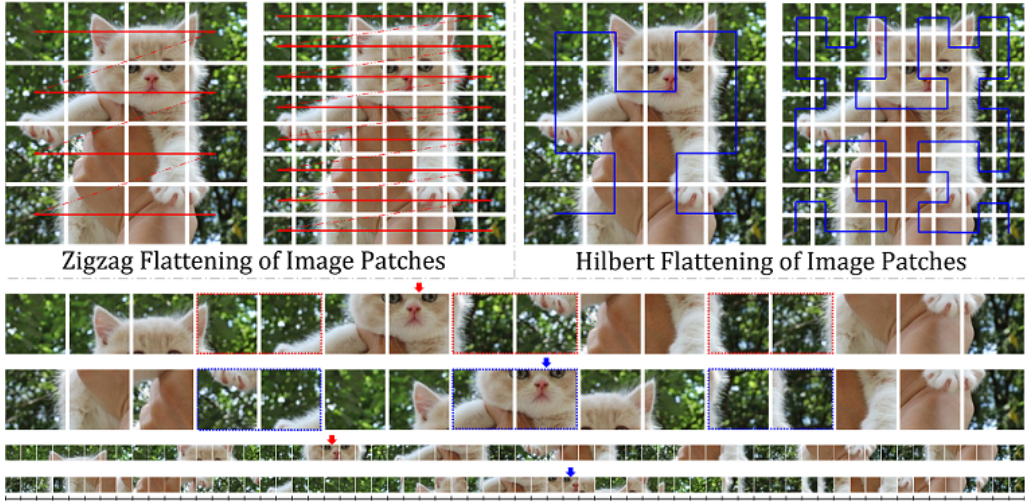


Figure 1: Zigzag flattening (red lines and arrows) VS. Hilbert flattening (blue lines and arrows) in ViT for image patch expanding. When flattening a 2D image into a 1D patch sequence, ZF will move the initially adjacent image blocks (semantically related patches) away from each other, but HF does not. That is, the head of cat remained clustered together after slicing at different flattening scales, and the position of the head on the 1D sequence was not change.

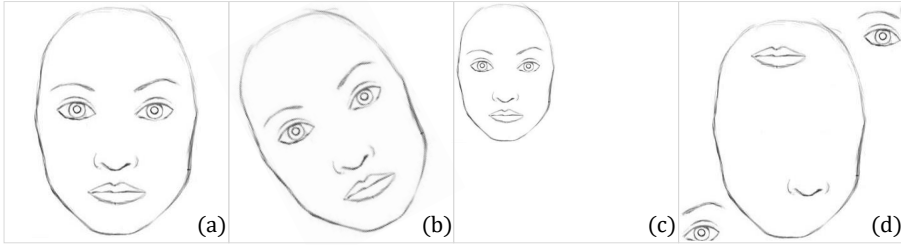


Figure 2: Illustration of Image Reading.

in the text must be fixed. If it was moved, the original message conveyed by the text would be subverted. This also explained that why the position encoding is prominent for Transformer to capture sequence ordering of input tokens. However, the key information of the image which consists of whole blocks of pixels would not change in any way even if it was moved by panning or scaling, see Fig. 2 (a) and (c). Notably, the feature points inside an image block can not be moved, just like the position of a keyword in a sentence. If the features were moved, the semantics expressed by the image would change radically, see Fig. 2 (a) and (d).

In the nutshell, there is a fundamental difference in the modality text and images represent information. Hence, it is naive to apply the mode of reading text directly to read images in CV. For this purpose, we investigated the Hilbert fractal flattening strategy (aka Pseudo-Hilbert curve flattening or “Hilbert” for short) as another method for image reading in CV and contrast it against ZF. The Hilbert is the only space-filling curve whose Hausdorff–Besicovitch dimension is greater than its topological dimension Albers & Alexanderson (2008). And it has been shown to outperform the other curves in remaining the spatial locality, when transforming from a multi-dimensional space to a one-dimensional space Moon et al. (2001). Several related works have applied it simply to the indexing of image pixels in CV. But, its theoretical explanation and application potential have not been well investigated, and even remains controversial.

In this paper, we first discussed the nature of the Hilbert fractal in image dimensional transformation and its scale robustness. Then, extensive experiments including Dynamic Time Warping (DTW) distance, interpolation based image resize, image classification, etc, demonstrated that Hilbert flattening was a better image reading method compared to “zigzag” flattening. Our contributions can be summarized as follows:

- We posed a simple but easily taken-for-granted question. In ViTs and MLPs, does the model have to use the same paradigm for reading images as it does for text reading? Through theoretical analysis and fine experimental design, we have attempted to give one answer and to generalize this question to a larger context.

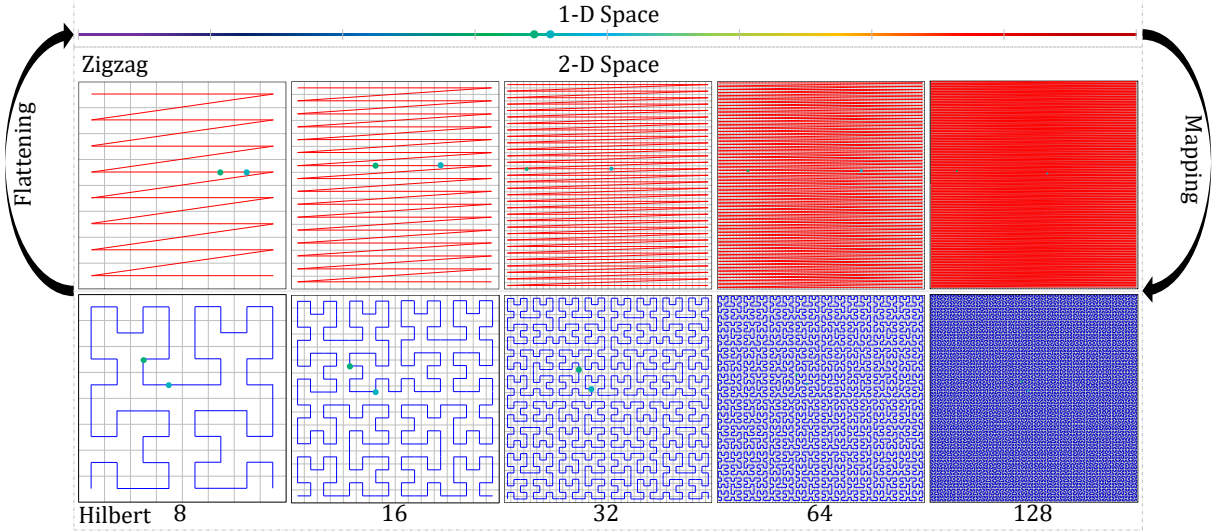


Figure 3: Multi-scale transformation of dimensional space with Zigzag flattening and Hilbert flattening, respectively.

- We answered previous controversial questions. We have theoretically estimated the square-to-linear dilation factor of the finite approximation of Hilbert curve. This indicates that the consecutive parts in sequence are close in the corresponding image, and explains that why Tsinganos et al. (2019) can feed the 1D signals to the CNNs. Meanwhile, The Average Square Distance was proposed to give a quantitative description of comparison between inverse Hilbert flattening and inverse Zigzag flattening on probability of points close in 2-dimension are close in linear sequence. In addition, we empirically demonstrate that the Hilbert flattening can maintain feature consistency in multi-scale images.
- We proposed a new patch embedding method, named Hilbert Patch Embedding (HPE), dedicated to any DNNs, considering both effectiveness and simplicity. The HPE are simple and can be easily plugged into most DNNs. Experiments demonstrate that, without introducing additional hyperparameters, it can improve ViT and the proposed Feature Pyramid Network (FPN-MLPs) by 0.53% (Top1 Acc) and 4.29% over their original models on ImageNet Deng et al. (2009) and CIFAR-10 Krizhevsky et al. (2014), respectively. Meanwhile, assume that the positions between two adjacent tokens are always close to each other, we proposed a regularity term for position encoding of Transformers based architectures.

## 2 Related Work

### 2.1 Space-Filling Curves

A continuous curve is called *space-filling curve* if it can pass through every point of a closed square Peano (1890). More precisely, a space-filling curve is a continuous mapping from a closed unit interval  $I = [0, 1]$  to a closed unit square  $Q = [0, 1]^2$  Simmons (1963). It is defined as follows:

**Definition 1** A mapping  $f: I \rightarrow E^n (n \geq 2)$  is continuous and  $f(I)$  has positive Peano–Jordan measure, then  $f(I)$  is called a space-filling curve, where  $E^n$  denotes an  $n$ -dimensional Euclidean space.

Hilbert curve Hilbert (1935) is the first generic geometric program that allows to construct entire classes of space-filling curves. Compared to zigzag curves and Gray-encoded curves, Hilbert curves were the best at minimizing the number of clusters Jagadish (1990).

### 2.2 Applications of Hilbert Curves

Such prominent works in the field of Mathematics as Jagadish (1990); Gotsman & Lindenbaum (1996); Moon et al. (2001) have evidenced that the locality between objects in multi-dimensional space is preserved in linear space. Inspired by such idea, recent widely works consist of Tsinganos et al. (2019); Bappy et al. (2019); Zhang et al. (2021) have been proposed to introduce the Hilbert curves into a CV application. Bappy et al. (2019) noted that the order of the

image patches has a significant impact on the performance of the Long-Short Term Memory (LSTM), and if the zigzag flattening was performed in the horizontal direction, the neighboring blocks in the vertical direction are far apart. Eventually, the LSTM may not establish the connection between those patches well. To improve the performance of localization in the detection of image forgeries, they utilized the Hilbert curves to arrange image patches before the block sequences were fed into the LSTM. With the same idea, to extract the better spatial features, FDPT Zhang et al. (2021) also utilized the Hilbert curves to flatten image patches before feed them into the Gated Recurrent Unit (GRU). By contrast, Tsinganatos et al. (2019) employed the Hilbert curves to generate 2D image representations from 1D surface electromyography (sEMG) signals, then the features of the sEMG signals were extracted by the CNN based backbones. But, the above methods only apply the Hilbert curve to a CV task without in-depth theoretical analysis and fine empirical experimental proofs.

### 2.3 ViTs and MLPs

Vision Transformer Dosovitskiy et al. (2021) inspires a new paradigm architecture that differs from CNNs by utilizing patch embedding instead of taking images directly as input. Pyramid Vision Transformer (PVT) Wang et al. (2021) extends ViT by employing the pyramid structure, and Swin Transformer Liu et al. (2021) proposes shifted windows to solve larger variations of the input image caused by the multi-scale and high resolution. By contrast, MLP-Mixer Tolstikhin et al. (2021) proposed a new architecture that differs from CNNs and Transformers by eliminating the need for convolution and self-attention, and relies only on the repeated implementations of multi-layer perceptron across the spatial or feature channels. With the same motivation, ResMLP Touvron et al. (2021) exploited the effect of data augmentation and knowledge distillation on training a MLPs based architecture. Those works above all employed the zigzag flattening to expand 2D images or features into 1D patch or pixel sequences. But the ZF would move the initially adjacent image blocks (semantically related patches) away from each other, but HF does not, see Fig. 1 for details. Hence, in this paper, we explored Hilbert curves whose cluster property outperform zigzag curves for those ViTs and MLPs based architectures.

## 3 Method

### 3.1 Preliminary

In this subsection we give a brief introduction of basic properties of the Hilbert curve purely on the basis of its definition by a geometric generating process. We denote  $\mathcal{I}$  and  $\mathcal{Q}$  as the interval  $[0, 1]$  and square  $[0, 1] \times [0, 1]$  respectively. In order to get a clear comprehension of generating of Hilbert curve by iteration process, we draw the iteration ( $3 \leq n \leq 7$ ) in Figure 3.

$$\begin{aligned} T_0 z &= \frac{1}{2} H_0 z + h_0, H_0 z = \bar{z}i, h_0 = 0 \\ T_1 z &= \frac{1}{2} H_1 z + h_1, H_1 z = z, h_1 = \frac{i}{2} \\ T_2 z &= \frac{1}{2} H_2 z + h_2, H_2 z = z, h_2 = \frac{1}{2} + \frac{i}{2} \\ T_3 z &= \frac{1}{2} H_3 z + h_3, H_3 z = -\bar{z}i, h_3 = 1 + \frac{i}{2} \end{aligned} \tag{1}$$

We call  $n$ -th iteration as the approximation of Hilbert curve of order  $n$ . As shown in Figure 3, we see that the order  $n$  approximation of Hilbert curve originates in the lower-left sub-square and terminates in the lower-right sub-square. The exit point from each sub-square coincides with the point which go into the following sub-square. In formal mathematical language, we can represent the iteration process by applying the above transformations (Equation 1) which utilize complex representation. Take transformation  $T_0$  as an example: with  $z \in \mathbb{C}$ , we first shrink the original  $\mathcal{Q}$  towards the original point under the ratio  $\frac{1}{2}$ . Then reflect on the imaginary axis by multiplying with  $-1$  and rotate the square through  $90^\circ$  by multiplying with  $i$ .

Given a real number  $t \in [0, 1]$  represented in quaternary form:

$$t = 0.q_1 q_2 \cdots, 0 \leq q_j \leq 3 \tag{2}$$

The Hilbert curve mapping between  $[0, 1]$  and  $[0, 1] \times [0, 1]$  is shown as

$$\mathcal{H}(t) = \begin{pmatrix} \mathcal{R}e \\ \mathcal{I}m \end{pmatrix} \lim_{n \rightarrow \infty} T_{q_1} T_{q_2} \cdots T_{q_n} \mathcal{Q} \tag{3}$$

As the order of Hilbert curve increases, the subsquares shrink into points, which claims that  $\mathcal{H}(t)$  is a point in  $\mathbb{R}^2$ . Moreover, for finite quaternaries which are end or beginning points of subintervals of partition of  $\mathcal{I}$ , we have

$$\begin{aligned}\mathcal{H}(t) &= \binom{\mathcal{R}e}{\mathcal{I}m} \sum_{j=1}^n \frac{1}{2^j} H_{q_0} H_{q_1} H_{q_2} \cdots H_{q_{j-1}} h_{q_j} \\ &= \sum_{j=1}^n \frac{1}{2^j} (-1)^{e_{0j}} \operatorname{sgn}(q_j) \binom{(1-d_j)q_j - 1}{1-d_j q_j} \\ \text{where } \operatorname{sgn}(x) &= \begin{cases} 1, & \text{if } x > 0, \\ 0, & x = 0 \end{cases}\end{aligned}\quad (4)$$

where  $H_{q_0}z = z$ ,  $e_{kj}$  is the number of  $k$ 's preceding  $q_j \pmod{2}$ ,  $d_j = e_{0j} + e_{3j} \pmod{2}$ , for  $k = 0, 3$ .

### 3.2 Dilation Bound

With the Hilbert curve representation, we can traverse every pixel in the image(square). One critical question is whether the relative position information of the pixels can be preserved under Hilbert curve. Before exploring the property of Hilbert curve, we recall the flatten operation which is common used in deep learning (especially compute vision).

Specifically, we always transform the  $H \times W \times C$  image/feature map into  $(H * W) \times C$  tensor by utilizing Zigzag flattening operation. The order of feature elements in flatten feature map belong to zigzag shape in the original feature map, which lead to the fact that contiguous patches in original feature map can be distant in flatten feature map. In order to preserve the relative position information and reduce the ambiguity we have to concern the conjunction part of flatten feature map specially. On the other hand, as shown in Equation 4, given two points  $t^1, t^2$  in the interval  $[0, 1]$ , we represent them in quaternary form:

$$\begin{aligned}t^1 &= 0.q_1^1 q_2^1 \cdots \\ t^2 &= 0.q_1^2 q_2^2 \cdots\end{aligned}\quad (5)$$

when these two points are close in interval, which means that for an large integer  $j$  such that  $q_k^1 = q_k^2, \forall 1 \leq k \leq j$ . By applying the formula in Equation 4, we obtain the distance between point of  $\mathcal{H}(t^1), \mathcal{H}(t^2)$  as follows:

$$|\mathcal{H}(t^1) - \mathcal{H}(t^2)|^2 \leq \left( \sum_{k=j+1}^{\infty} \frac{1}{2^k} * 8 \right) \leq \frac{8}{2^j} \quad (6)$$

Moreover, the dilation bound of HF is estimated in Bauman (2006),

**Theorem 1** *The square-to-linear dilation factor of the Peano-Hilbert curve is equal to 6, which means that the maximum value of  $\frac{|\mathcal{H}(t^1) - \mathcal{H}(t^2)|^2}{|t^1 - t^2|} \leq 6$ .*

The HF operation can obtain an sequence ordering of the image/feature map which guarantee that consecutive parts in sequence are close in original image.

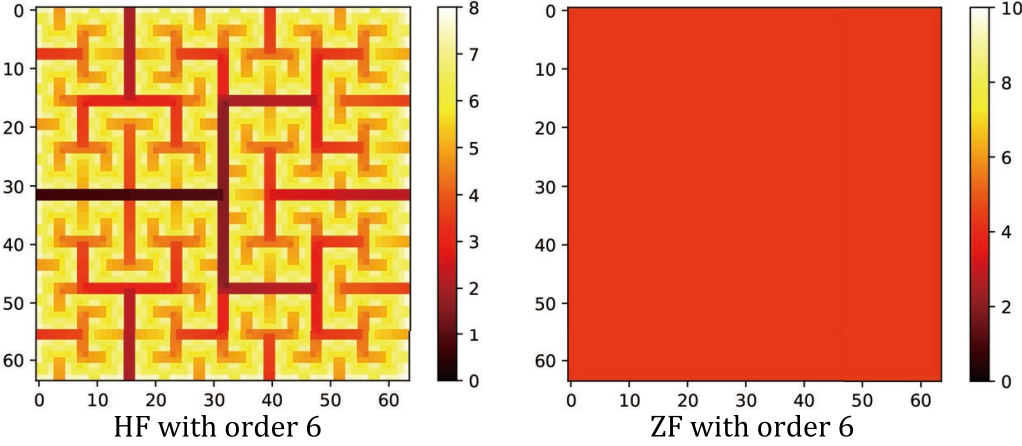
**Dilation Bound of ZF** Given a real number  $t \in [0, 1]$  represented in quaternary form:  $t = 0.q_1 q_2 \cdots q_n$ , the ZF map the interval  $[0, 1]$  to  $[0, 1] \times [0, 1]$  in the following form:

$$\mathcal{Z} : 0.q_1 q_2 \cdots q_n \mapsto \left( \begin{array}{l} \left( \sum_{i=1}^n q_i 4^{n-i} \% 2^n \right) * \frac{1}{2^n} + \frac{1}{2^{n+1}} \\ \left( \sum_{i=1}^n q_i 4^{n-i} \right) * \frac{1}{2^n} + \frac{1}{2^{n+1}} \end{array} \right) \quad (7)$$

when we choose  $t^1 = 0.\underbrace{00 \cdots 0}_{n-2} 10$  and  $t^2 = 0.\underbrace{00 \cdots 0}_{n-2} 11$ , they are consecutive points in the interval  $[0, 1]$  with distance  $\frac{1}{4^n}$ . Then we have  $|\frac{\mathcal{Z}(t^1) - \mathcal{Z}(t^2)|^2}{\frac{1}{4^n}} = \frac{(1 - \frac{1}{2^n})^2 + \frac{1}{4^n}}{\frac{1}{4^n}} = 4^n - 2^{n+1} + 2$ . We draw the conclusion ZF operation obtain a sequence ordering of the image/feature map where consecutive points are distant in original image.

Table 1: The percentage of points with given  $ASD^{\frac{1}{2}}$  threshold.

$ASD^{\frac{1}{2}}$	1.4000e-2	1.3778e-2	1.3556e-2	1.3333e-2	1.3111e-2	1.2889e-2	1.2667e-2	1.2444e-2	1.2222e-2	1.2000e-2
ZF	100.00%	96.97%	96.97%	3.13%	3.13%	3.13%	3.08%	3.03%	3.03%	0.00%
HF	80.57%	80.57%	80.57%	80.57%	80.57%	79.54%	78.76%	78.76%	78.76%	76.71%

Figure 4: The heatmap of  $-\log ASD^{\frac{1}{2}}$ ,

### 3.3 Inverse Hilbert Flattening

Sequence ordering will change the original structure of image/feature map to some extent, it is essential to explore to what extent HF/ZF can preserve the original two dimensional structure. First we denote the inverse map of HF as

$$\mathcal{F}^{-1} : \left( \begin{array}{c} \frac{i}{2^n} + \frac{1}{2^{n+1}} \\ \frac{j}{2^n} + \frac{1}{2^{n+1}} \end{array} \right) \mapsto = 0.q_1q_2 \cdots q_n \quad (8)$$

where  $q_{i+1} = \lfloor \frac{j*2^n - \sum_{k=1}^i q_k * 4^{n-k}}{4^{n-i-1}} \rfloor$  and  $q_1 = \lfloor \frac{j*2^n}{4^{n-1}} \rfloor$ . For each pixel  $p$  at position  $(i, j)$ , we consider the neighbors which are  $K$  steps away from  $p$ . We calculate the Average Square distance (ASD) of those pixels respect to  $p$  as follows:

$$ASD(p) = \frac{\sum_{k=i-K}^{i+K} \sum_{l=j-K}^{j+K} (\mathcal{F}^{-1}(p_{kl}) - \mathcal{F}^{-1}(p))^2}{\#(\text{neighbors})} \quad (9)$$

As shown in Figure 4, most points have a uniform high ASD value under ZF mechanism, while over a certain percentage of points in HF have a small ASD value. Moreover, we give an quantitative comparison between ZF and HF (order 6) on percentage of points whose  $ASD^{\frac{1}{2}}$  is smaller than a given threshold.

### 3.4 Scale Robustness

Take  $\Omega = \mathbb{Z}_{2^n} \times \mathbb{Z}_{2^n}$  to be a two-dimensional  $2^n \times 2^n$  grid, given an RGB image as an mapping :  $\Omega \rightarrow \mathbb{R}^3$ . As proposed by Bronstein et al. (2021), the convolutional layers of CNNs are shift-equivariant. The general equivariant is defined as follows,

**Definition 2** A function  $f : \mathcal{X}(\Omega) \rightarrow \mathcal{X}(\Omega)$  is  $\mathcal{G}$ -equivariant if  $f(\rho(g)x) = \rho(g)f(x)$  for all  $g \in \mathcal{G}$ , i.e., group action on the input affects the output in the same way, where  $\mathcal{X}(\Omega)$  denotes all signals on domain  $\Omega$ .

**Definition 3** A function  $f : \mathcal{X}(\Omega) \rightarrow \mathcal{X}(\Omega)$  is  $\mathcal{G}$ -robust if  $f(\rho(g)x) \approx \rho(g)f(x)$  for all  $g \in \mathcal{G}$ , i.e., group action on the input affects the output in the same way, where  $\mathcal{X}(\Omega)$  denotes all signals on domain  $\Omega$ .

Consider the  $n$ -th order and  $(n + 1)$ -th order approximation of Hilbert curve mapping.

$$\begin{aligned} 0.q_1q_2 \cdots q_n &\mapsto \sum_{j=1}^n \frac{1}{2^j} (-1)^{e_{0j}} \operatorname{sgn}(q_j) \binom{(1-d_j)q_j - 1}{1-d_jq_j} \\ 0.q_1q_2 \cdots q_nq_{n+1} &\mapsto \sum_{j=1}^{n+1} \frac{1}{2^j} (-1)^{e_{0j}} \operatorname{sgn}(q_j) \binom{(1-d_j)q_j - 1}{1-d_jq_j} \end{aligned} \quad (10)$$

Geometrically, the above operation just divide the  $n$ -th order approximation Hilbert curve uniformly between every pair of end points into three parts, then move the second part away from the original curve with distance  $\frac{1}{2^{n+1}}$ . Finally connect the moved part with the end points of the second part. (See Figure 3 with  $n = 3$  and  $n = 4$ ). Given an image  $I$  with size  $2^{n+1} \times 2^{n+1}$ , we utilize the  $n + 1$ -th order HF to flatten it. We denote the image/feature after flattening as  $\mathcal{H}_{n+1}(I)$ . On the other hand, we scale(downsampling) the image  $I$  into image  $I_{\frac{1}{2}}$  with size  $2^n \times 2^n$ . We denote the image/feature after  $n$ -th order HF as  $\mathcal{H}_n(I_{\frac{1}{2}})$ . As common sense, adjacent pixels usually contains similar information, with high probability,  $\mathcal{H}_n(I_{\frac{1}{2}})$  and  $\mathcal{H}_{n+1}(I)$  satisfies following condition:

$$(\mathcal{H}_{n+1}(I))_{\frac{1}{2}} \approx \mathcal{H}_n(I_{\frac{1}{2}}) \quad (11)$$

Here  $\frac{1}{2}$  means that scale (downsample) with ratio  $\frac{1}{2}$ . Consider the scale operation group  $\mathcal{S} = \{2^{-m} | m \in \mathbb{Z}\}$ , we have

$$(\mathcal{H}_{n+m}(I))_{2^{-m}} \approx \mathcal{H}_n(I_{2^{-m}}) \quad (12)$$

In conclusion, as  $n$  approach a sufficiently large number (infinity), we get the Hilbert curve mapping is  $\mathcal{S}$ -robust.

## 4 Experiments

In this section, two analysis experiments were first reported to compare the scale robustness of ZF and HF. Second, a FPN-MLPs architecture was proposed to compare the multi-scale representations stability of both. Third, We introduce an implementation of patch embedding (HPE) for the Transformer based architectures, see Fig. 1, which sets the flattening strategy between image patches and the patch pixels, separately. Finally, we proposed a regularity term for position encoding of ViTs, and the related experiments validated that HF could yield effective benefits in position embedding. In addition, the impact of patch size on the performance of ZF and HF is analysed.

**Experimental Setup.** For self-consistent, we utilized the same networks in all baseline settings to compare the performance. Notably, we only control the variable of flattening methods in any experiments, and other settings including software and hardware are strictly consistent.

### 4.1 Scale Robustness

**Dynamic Time Warping Distance.** Dynamic time warping (DTW) is a prominent approach to obtain an optimal alignment between two given (One-Dimension) sequences under certain restrictions Berndt & Clifford (1994). Initially, DTW was commonly utilized to compare different speech modalities in automatic speech recognition, see Müller (2007). Here, we produced a demo dataset consists of three common shape (circle, square and triangle), see details in Appendix. All the images are first flattened into a one-dimensional form by two different unfolding strategies (HF VS. ZF, see Fig. 3), and then the DTW distance between any two images is calculated. The detailed results are reported in Table 2. When the resolution of the two images is equal, turn up the resolution, the DTW distance between large and small targets will also follow the increase. However, The change of DTW value in HF is very small compared to ZF. When the target scale of the two images is equal, turn up the resolution of both, the DTW distance between different resolutions will also follow the increase. HF is still the method with the least variation in DTW values. In addition, the DTW value of HF is always the smallest one among all settings, and at the smallest it is only one-fifth of ZF.

**Image Scaling.** Image scaling is a common operation in digital image processing (DIP). Two interpolations by row and column respectively are the standard practice for image scaling. But, if we expand the image and interpolate it only once, will this scale the image properly? As shown in Fig. 5 (a) and (b), with ZF method, neither up-sampling nor down-sampling operations result in a normal image. On the contrary, with HF strategy, see Fig. 5 (c) and (d), the normal results are obtained regardless of the upsampling or downsampling operation. Moreover, the scaling effect of HF can perform favorably against the result of 2D interpolation algorithms.

Table 2: The DTW distance for different target sizes and image resolutions. Lower is better. (“L32” means Large scale image with a resolution of  $32 \times 32$  and “S32” means Small scale image with a resolution of  $32 \times 32$ .)

Scale Methods	L32 VS. S32		L32 VS. L64		L64 VS. S64		L64 VS. L128		L128 VS. S128		L32 VS. S128	
	HF	ZF	HF	ZF	HF	ZF	HF	ZF	HF	ZF	HF	ZF
Circle	5.19	8.61	4.13	14.32	6.14	16.28	6.74	28.71	9.13	33.31	<b>3.95</b>	18.52
Square	<b>3.40</b>	8.14	5.42	17.16	6.60	15.53	7.39	35.47	10.58	31.03	8.67	29.67
Triangle	4.61	9.60	<b>3.63</b>	16.03	6.93	18.83	6.06	31.55	7.99	38.07	4.30	10.28

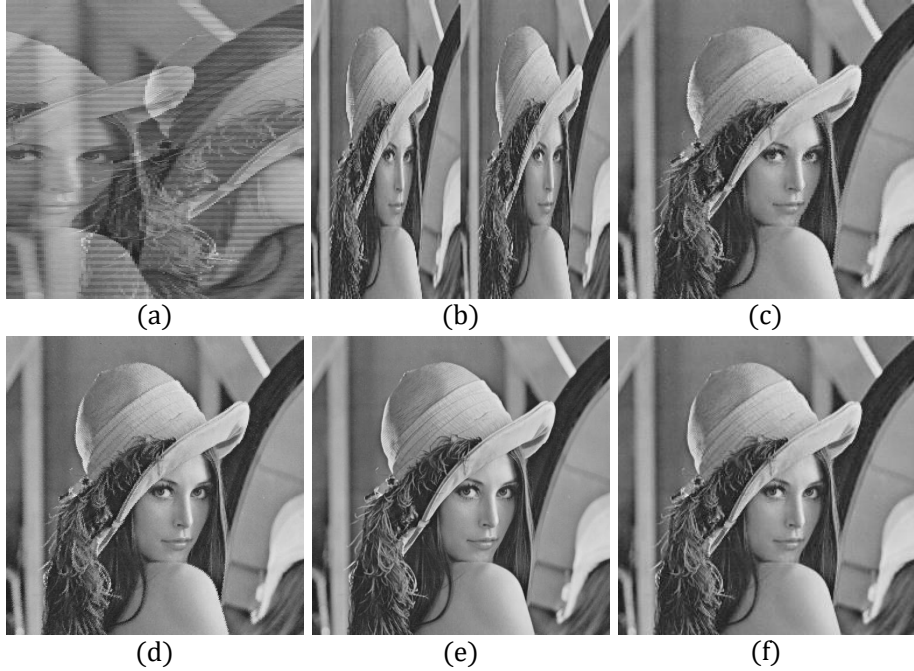


Figure 5: Qualitative results of the 1D interpolation-based image scaling. (a) After expanding the image from 2D to 1D with ZF, we downsample the original image to  $256 \times 256$  by the nearest neighbor 1D interpolation algorithm. (b) Again, we do the dimensional transform with ZF first, upsample the original image to  $512 \times 512$  by the same algorithm. (c) Same as (a), but with HF. (d) Same as (b), but with HF. (e)  $512 \times 512$  resolution original “Lena” image. (f)  $256 \times 256$  resolution original image.

## 4.2 Multi-scale Representations

The stability of multi-scale representations played a significant role in image recognition tasks Gao et al. (2019). To prove that better scale robustness can enhance the stability of multi-scale representations, an image pyramid structure based MLPs architecture was proposed, turn to Fig. 6 and Appendix for details. We conduct experiments on a general image classification datasets: CIFAR-10, which consists of  $60K$  images in 10 classes with  $6K$  images per class, and employed the commonly used protocols with the data augmentation Lee et al. (2015).

Table 3 presents the results of different flattening methods on CIFAR-10. The flattening method of “Residual-H-Backbone-H” can outperform the baseline of “Residual-Z-Backbone-Z” by obvious margins (4.29%, which are notable improvements). Regardless of any branch of the architecture, HF can widely improve the baseline performance of ZF. Notably, the performance impact of HF is greater on the image pyramid structure than on the backbone. That is, compared to ZF, HF can provide a stronger stability of multi-scale representations for the model.

In addition, with the setting of “Residual-H-Backbone-H”, the impact of different data augmentation methods on the performance of HF was explored. As reported in Table 4, the best result was obtained with the simple augmentation of “Resize”. “CenterCrop” could make the local information of the image lost, which may be the cause of its performance degradation. This also indicates the importance of residual branch to the performance of the proposed FPN-MLPs.

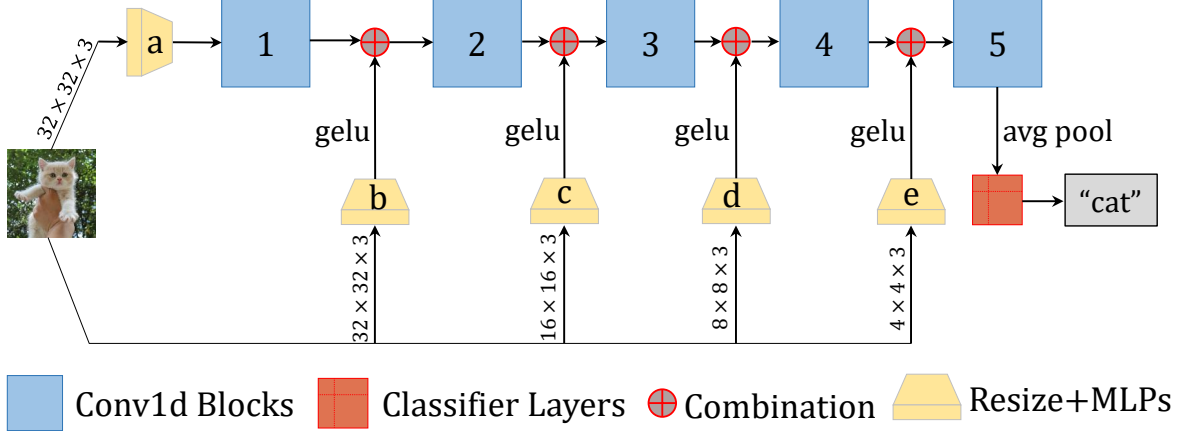


Figure 6: The pipeline of proposed FPN-MLPs architecture. The FPN-MLPs consists of the residual branch and a backbone network. The residual branch including an image pyramid structure and MLPs. The backbone is made up entirely of MLPs.

Table 3: On CIFAR-10, recognition accuracy of different flattening methods with the proposed FPN-MLPs. “Residual-H-Backbone-Z” indicates that the flattening approaches in the residual branch and backbone are HF and ZF, respectively. Same for the other settings.

Flattening Methods	Top-1%	Top-5%
Residual-Z-Backbone-Z	81.42	99.18
Residual-H-Backbone-Z	85.45	99.54
Residual-Z-Backbone-H	81.67	99.14
Residual-H-Backbone-H	<b>85.71</b>	99.58

Table 4: With the setting of “Residual-H-Backbone-Z”, recognition accuracy of different data augmentation on CIFAR-10.

Transforms	Top-1%	Top-5%
Resize	<b>85.71</b>	99.58
RandomCrop	85.28	99.50
RandomResizeCrop	85.40	99.56
CenterCrop	84.13	99.34

### 4.3 Hilbert Patch Embedding

To answer the proposed question that whether the ZF is the optimal solution for image reading of ViTs. A new patch embedding method named Hilbert patch embedding (HPE) was proposed for Transformer based architectures. As shown in Fig.1, HPE indicates that by utilizing the Hilbert flattening strategy for image patches embedding. Such two popular models as MLP-Mixer and ViT were employed by us to perform a series of experiments on the ImageNet1K and CIFAR-10 for image classification.

**MLP-Mixer.** Both convolution-free and attention-free model MLP-Mixer, which is an architecture based exclusively on MLPs. Similar to ViT, it also treats an image as  $16 \times 16$  words. That is, the patch embedding was an essential component of this model. As shown in Table 5, we conduct numerous experiments with different patch embedding approaches on CIFAR-10 by utilizing the MLP-Mixer. The results note that the proposed HPE is effective in MLP-Mixer and also achieves significant improvement based on the original patch embedding method. In addition, a 1D convolution based patch embedding method was proposed to compare HF and ZF. The experiments demonstrated that there is a obvious gap between the best accuracy of HF and ZF. Notably, when we utilized the overlap convolution, this gap was widened.

Table 5: Recognition accuracy of different patch embedding methods on CIFAR-10. “Inter-Z Intra-H” means that the flattening strategy in the inter-patches and intra-patches are ZF and HF, respectively. Same for the other settings. “Conv1D-H” indicates that encoding the image patches by the 1D convolution, and the flattening method of image patches is HF. “Conv1D-Z” means that the flattening method of image patches is ZF. “Overlap” indicates that the kernel size of Conv1D is bigger than the patch size.

Methods	Patch Size	Overlap	Top-1%	Top-5%
Original	8	-	87.05	99.15
Inter-H Intra-Z	8	-	<b>87.35</b>	99.19
Inter-Z Intra-Z	8	-	86.74	99.16
Inter-Z Intra-H	8	-	86.86	99.08
Inter-H Intra-H	8	-	86.75	99.18
Conv1D-Z	8	-	83.58	98.71
Conv1D-H	8	-	<b>84.52</b>	98.83
Conv1D-Z	4	-	79.73	98.34
Conv1D-H	4	-	<b>80.59</b>	98.55
Conv1D-Z	4	✓	80.48	98.32
Conv1D-H	4	✓	<b>81.68</b>	98.57

Table 6: Recognition accuracy of different patch embedding methods on ImageNet1K With the ViT-T/16 model.

Methods	Top-1%	Top-5%
Original	70.38	88.75
Inter-H Intra-Z	70.83	89.13
Inter-Z Intra-H	<b>70.91</b>	89.22
Inter-Z Intra-Z	70.63	88.92

**ViT.** To further demonstrate the generalizability of the proposed HPE, we employed the settings of ViT-T/16 in Dosovitskiy et al. (2021) to perform some experiments on ImageNet1K. ImageNet-1K (1K-class) consists of  $\sim 1.28M$  images for training and 50K validation images. We conduct experiments by utilizing the same comparison protocols and data augmentation as Radosavovic et al. (2020). The detailed results are reported in Table 6. With the setting of “Inter-H Intra-Z”, HPE is superior to the baseline of original patch embedding by 0.45%. Especially with the setting of “Inter-Z Intra-H”, HPE can further improve the accuracy of baseline from 70.38% to 70.91%. For self-consistency, the result of “Inter-Z Intra-Z” was also reported in Table 6. We note that there is still a clear gap between the accuracy of HF and ZF.

#### 4.4 Position Encoding Regularity

The basic component of transformer is self-attention Vaswani et al. (2017), which has a ability to model a relationship between the tokens in a sequence. But, It has an inherent defect, i.e., self-attention can not obtain the ordering of input tokens. So, position encoding was vital for the Transformer to capture the sequence orderings.

As introduced before, the positions between two adjacent tokens in an image are always close to each other. Inspired by this hypothetical, a regularity term for position encoding of ViTs was proposed to evidence that there is a gap of spatial locality between HF and ZF. One image patch was embedded to a token vector, all the input tokens formed the patch embedded vector. As shown in Fig. 7, the dimensionality of the associated position encoding vector is equal to patch embedded vector. The temperature parameters was proposed to enhance the positional encoding capability. Employing the temperature coefficients to update the weights of the position encoding vector, this process can be described by the Equation 13 below.

$$Token'_i = Token_i + T_{i-1} * Token_{i-1} + T_{i+1} * Token_{i+1}, \quad (13)$$

where  $i \in [2, M - 1]$ , “ $Token$ ” denotes the position encoding vector of a patch.

We employed the settings of ViT-T/8/4/2 in Dosovitskiy et al. (2021) to conducted extensive experiments on CIFAR-10. As reported in Table 7, regardless of the patch size, the proposed position encoding regularity could achieve a significant improvement based on the original patch embedding and the proposed HPE. That is, our position encoding regularity is effective in position encoding of ViT. With the setting of “Inter-H Intra-Z”, we note that the different patch size have a

Table 7: The effect of patch size and the proposed regular terms on the recognition accuracy of different patch embedding methods on CIFAR-10 .

Methods	Regular	Patch Size	Top-1%	Top-5%
Original	-	2	83.85	99.00
Original	✓	2	85.25	99.08
Inter-H Intra-Z	-	2	<b>86.32</b>	99.15
Inter-H Intra-Z	✓	2	85.71	99.10
Original	-	4	88.84	99.46
Original	✓	4	88.57	99.37
Inter-H Intra-Z	-	4	87.92	99.49
Inter-H Intra-Z	✓	4	88.82	99.53
Original	-	8	83.73	98.93
Original	✓	8	83.17	98.79
Inter-H Intra-Z	-	8	82.44	98.70
Inter-H Intra-Z	✓	8	<b>83.82</b>	98.70

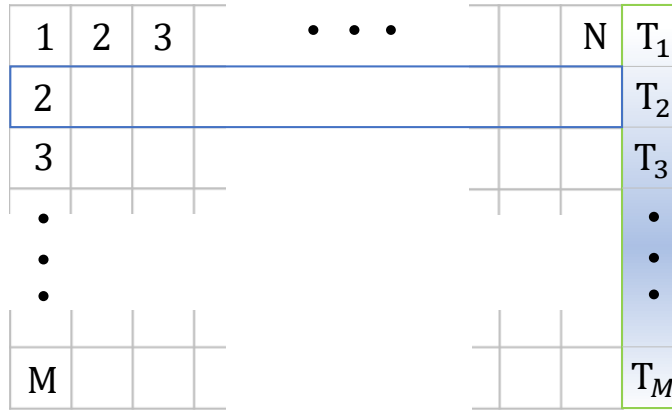


Figure 7: The gray table indicates the original position encoding vector ( $M \times N$ ). “M” and “N” indicates the number of patches and the length of embedded vector. “T” denotes a set of learnable temperature parameters, which is our proposed regularity term for position encoding of ViTs. The position encoding vector is updated with the weights by the action of temperature parameters  $T$ .

clear impact on the performance of both patch embedding methods. When the patch size was 2 or 8, with proposed position encoding regularity, HPE can obviously boost the performance over the baseline. Only when the patch size was 4, the proposed HPE does not achieve a lead.

## 5 Conclusion

In this paper, we explored whether Hilbert flattening is a better fit for image reading than Zigzag flattening. To answer the above question, we theoretically evaluate the square-to-linear dilation factor of the finite approximation of Hilbert curve, and propose the Average Square Distance to compare inverse HF with ZF. Based on the above theory, we proposed a new patch embedding method and a position encoding regularity for ViTs and MLPs. Extensive experiments including dynamic time warping distances, interpolation based image resize, and image classification demonstrate that HF is more effective than ZF.

## References

Abel, D. J. and Mark, D. M. A comparative analysis of some two-dimensional orderings. *International Journal of Geographical Information Systems*, 4(1):21–31, 1990.

Albers, D. J. and Alexanderson, G. L. Benoît mandelbrot: In his own words. *Mathematical people: profiles and interviews*. Wellesley, MA: AK Peters, pp. 214, 2008.

Bappy, J. H., Simons, C., Nataraj, L., Manjunath, B. S., and Roy-Chowdhury, A. K. Hybrid LSTM and encoder-decoder architecture for detection of image forgeries. *IEEE Trans. Image Process.*, 28(7):3286–3300, 2019.

Bauman, K. The dilation factor of the peano-hilbert curve. *Mathematical Notes*, 80:609–620, 11 2006.

Berndt, D. J. and Clifford, J. Using dynamic time warping to find patterns in time series. In *KDD workshop*, volume 10, pp. 359–370. Seattle, WA, USA:, 1994.

Bronstein, M. M., Bruna, J., Cohen, T., and Veličković, P. Geometric deep learning: Grids, groups, graphs, geodesics, and gauges, 2021.

Chen, S., Xie, E., Ge, C., Liang, D., and Luo, P. Cyclemlp: A mlp-like architecture for dense prediction. *CoRR*, abs/2107.10224, 2021.

Deng, J., Dong, W., Socher, R., Li, L.-J., Li, K., and Fei-Fei, L. Imagenet: A large-scale hierarchical image database. In *CVPR*, pp. 248–255. Ieee, 2009.

Dosovitskiy, A., Beyer, L., Kolesnikov, A., Weissenborn, D., Zhai, X., Unterthiner, T., Dehghani, M., Minderer, M., Heigold, G., Gelly, S., Uszkoreit, J., and Houlsby, N. An image is worth 16x16 words: Transformers for image recognition at scale. In *9th International Conference on Learning Representations, ICLR 2021, Virtual Event, Austria*, 2021.

Gao, S., Cheng, M.-M., Zhao, K., Zhang, X.-Y., Yang, M.-H., and Torr, P. H. Res2net: A new multi-scale backbone architecture. *IEEE transactions on pattern analysis and machine intelligence*, 2019.

Gotsman, C. and Lindenbaum, M. On the metric properties of discrete space-filling curves. *IEEE Trans. Image Process.*, 5(5):794–797, 1996.

Hilbert, D. Über die stetige abbildung einer linie auf ein flächenstück. In *Dritter Band: Analysis· Grundlagen der Mathematik· Physik Verschiedenes*, pp. 1–2. Springer, 1935.

Jagadish, H. V. Linear clustering of objects with multiple attributes. In *Proceedings of the 1990 ACM SIGMOD International Conference on Management of Data, Atlantic City, NJ, USA*, pp. 332–342. ACM Press, 1990.

Krizhevsky, A., Nair, V., and Hinton, G. The cifar-10 dataset. *online: <http://www.cs.toronto.edu/kriz/cifar.html>*, 55 (5), 2014.

Lee, C.-Y., Xie, S., Gallagher, P., Zhang, Z., and Tu, Z. Deeply-supervised nets. In *Artificial intelligence and statistics*, pp. 562–570. PMLR, 2015.

Liu, Z., Lin, Y., Cao, Y., Hu, H., Wei, Y., Zhang, Z., Lin, S., and Guo, B. Swin transformer: Hierarchical vision transformer using shifted windows. In *ICCV*, 2021.

Moon, B., Jagadish, H. V., Faloutsos, C., and Saltz, J. H. Analysis of the clustering properties of the hilbert space-filling curve. *IEEE Trans. Knowl. Data Eng.*, 13(1):124–141, 2001.

Müller, M. Dynamic time warping. *Information retrieval for music and motion*, pp. 69–84, 2007.

Peano, G. Sur une courbe, qui remplit toute une aire plane. *Mathematische Annalen*, 36(1):157–160, 1890.

Radosavovic, I., Kosaraju, R. P., Girshick, R., He, K., and Dollár, P. Designing network design spaces. In *CVPR*, 2020.

Simmons, G. F. *Introduction to topology and modern analysis*, volume 44. Tokyo, 1963.

Tolstikhin, I. O., Houlsby, N., Kolesnikov, A., Beyer, L., Zhai, X., Unterthiner, T., Yung, J., Steiner, A., Keysers, D., Uszkoreit, J., Lucic, M., and Dosovitskiy, A. Mlp-mixer: An all-mlp architecture for vision. *CoRR*, abs/2105.01601, 2021.

Touvron, H., Bojanowski, P., Caron, M., Cord, M., El-Nouby, A., Grave, E., Joulin, A., Synnaeve, G., Verbeek, J., and Jégou, H. Resmlp: Feedforward networks for image classification with data-efficient training. *CoRR*, abs/2105.03404, 2021.

Tsinganos, P., Cornelis, B., Cornelis, J., Jansen, B., and Skodras, A. A hilbert curve based representation of semg signals for gesture recognition. In *International Conference on Systems, Signals and Image Processing, IWSSIP 2019, Osijek, Croatia, June 5-7, 2019*, pp. 201–206. IEEE, 2019.

Vaswani, A., Shazeer, N., Parmar, N., Uszkoreit, J., Jones, L., Gomez, A. N., Kaiser, Ł., and Polosukhin, I. Attention is all you need. In *Advances in neural information processing systems*, pp. 5998–6008, 2017.

Wang, W., Xie, E., Li, X., Fan, D., Song, K., Liang, D., Lu, T., Luo, P., and Shao, L. Pyramid vision transformer: A versatile backbone for dense prediction without convolutions. In *ICCV*, 2021.

Zhang, X., Wang, S., Liu, C., Zhang, M., Liu, X., and Xie, H. Thinking in patch: Towards generalizable forgery detection with patch transformation. In *PRICAI 2021: Trends in Artificial Intelligence - 18th Pacific Rim International Conference on Artificial Intelligence*, volume 13033, pp. 337–352, 2021.

## 6 Appendix

### 6.1 Illustration of the demo dataset for Multi-scale Representations

The demo dataset for multi-scale representations is shown in Figure 8.

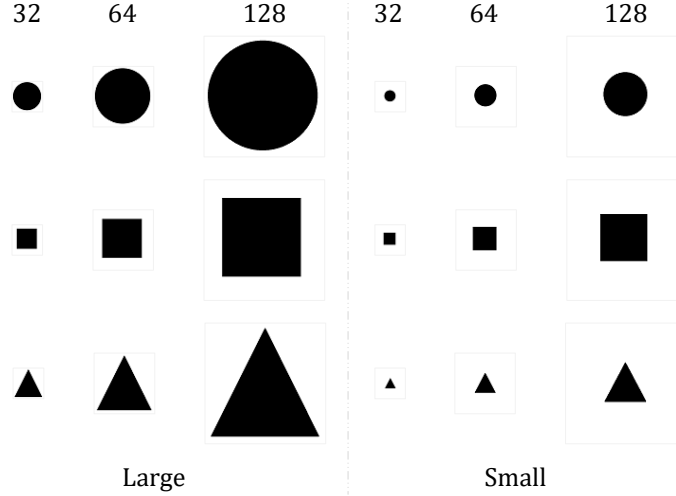


Figure 8: Three common image shapes including “circle”, “square” and “triangle” are generated. Each shape consists of three resolutions ( $32 \times 32$ ,  $64 \times 64$ ,  $128 \times 128$ ) and two target scales (large and small).

### 6.2 Outline of the proposed network architecture FPN-MLPs

The outline of the proposed network architecture FPN-MLPs is shown in Table 8.

Table 8: The outline of the proposed network architecture FPN-MLPs. The output size of each block is the input size of the next one see Fig. 6. From top to bottom, the components appear in sequence. Each component may appear multiple times in FPN-MLPs.

Type	Patch size/Stride or Remarks	Input Size
Conv1D	$7 \times 1/1$	$3 \times 1024$
Conv1D	$5 \times 1/2$	$64 \times 256$
Conv1D	$3 \times 1/2$	$256 \times 64$
Conv1D	$3 \times 1/2$	$512 \times 16$
Conv1D	$3 \times 1/1$	$3 \times 1024/256/64/16$
Conv1D	$1 \times 1/1$	$3 \times 1024/256/64/16$
GELU	$3 \times 1/1$	$3 \times 1024/256/64/16$
LayerNorm	$3 \times 1/1$	$3 \times 1024/256/64/16$
AvgPool1D	$16 \times 1$	$512 \times 16$
Linear	<i>Logits</i>	$1 \times 512$
Softmax	<i>Classifier</i>	$1 \times 10$